Supplement of Earth Surf. Dynam., 14, 763–780, 2026
https://doi.org/10.5194/esurf-14-763-2026-supplement
© Author(s) 2026. CC BY 4.0 License.

Earth Surface Dynamics
Open Access
EGU

Supplement of

Long-term peat thickness from cosmogenic ^{26}Al and ^{10}Be, Hautes Fagnes, Belgian Ardennes

Angus Moore et al.

Correspondence to: Angus Moore (moore@ig.cas.cz)

The copyright of individual parts of the supplement might differ from the article licence.

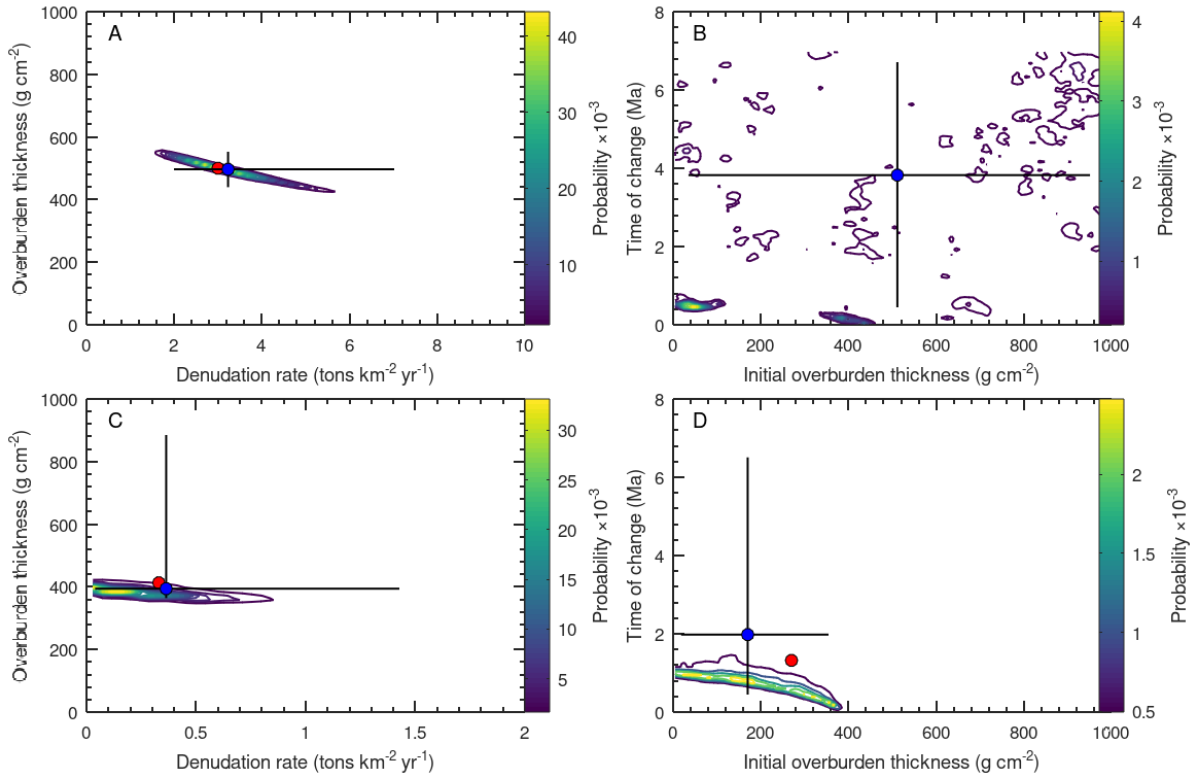

Figure S.1: Joint-distribution plots for two test-cases of the Markov Chain Monte Carlo (MCMC) inversion (main text, section 3.5.4). Red circles show the target parameter values. Blue circles and error bars show the median parameter estimate and 90% confidence interval from the MCMC inversion. Panels A and B show inversion results for a denudation rate of 3 tons km^{-2} yr^{-1} and an overburden thickness of 500 g cm^{-2}, with no change in overburden thickness with time, modeled using Eq. 5. The inversion successfully recovers the target denudation rate and overburden thickness (Panel A), while the timing of the change in overburden thickness and the initial thickness remain unconstrained (Panel B). Panels C and D show the inversion for median parameter values similar to those obtained for LS1 as targets (main text, Table 2). The model returns the parameter values within the 90% confidence interval, although with a greater offset between the median solution and the target values than achieved in the simpler case of no change in overburden thickness (Panel A).

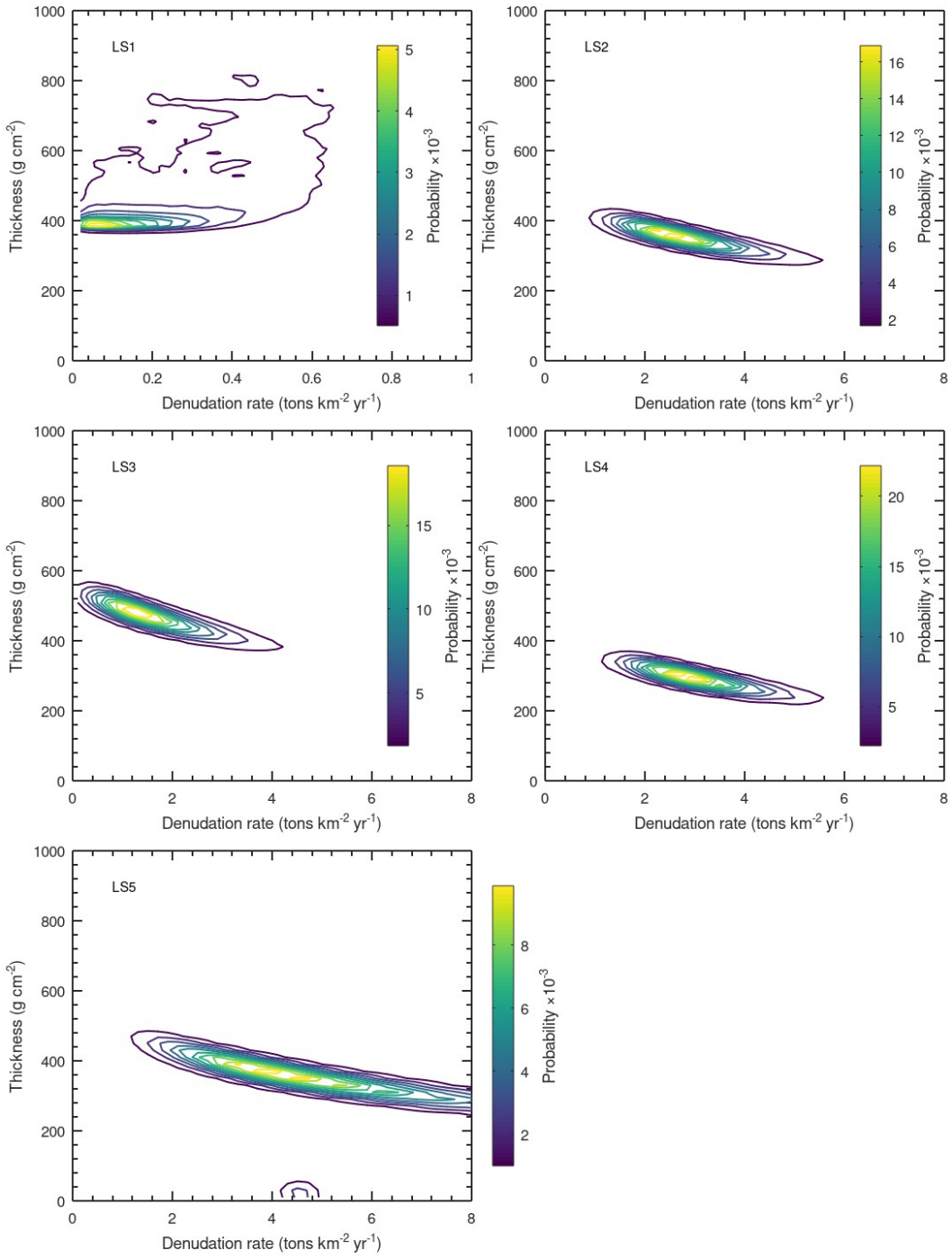

Figure S.2: Joint-distribution plots of the denudation rate vs. overburden thickness for the five hillslope positions (LS1-LS5). The thicknesses are not corrected for the depth between the peat/mineral soil interface and the sample. The overburden thicknesses and denudation rates generally covary negatively.

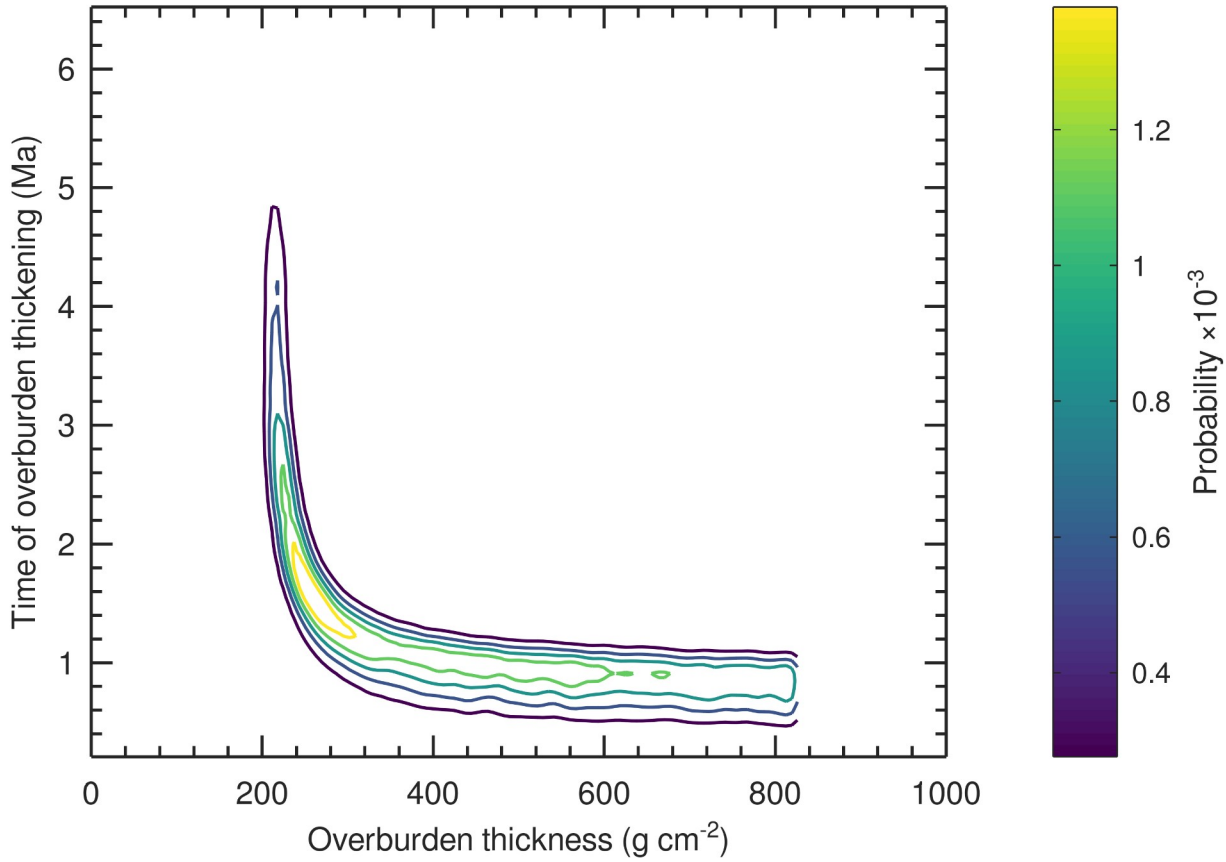

Figure S.3: Joint-distribution plot of the overburden thickness after the change in thickness vs. the time of the change inferred from the hillslope model (main text, Eq. 5) for LS1. Ages greater than ca. 1.4 Ma are allowable only at the lowest overburden thicknesses.

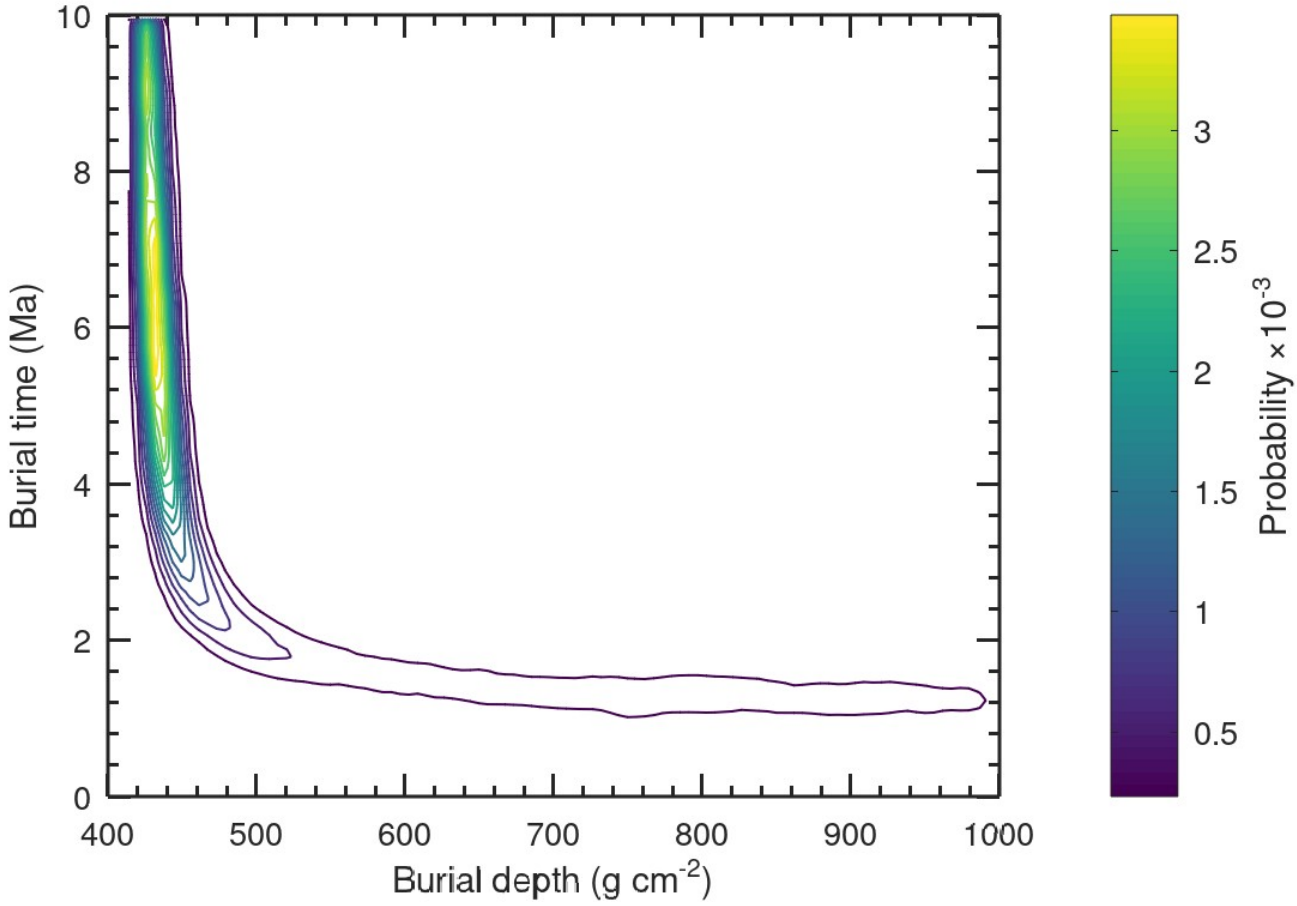

Figure S.4: Joint-distribution plot of the burial depth vs. burial time inferred from the valley-bottom sediment model (main text, Eq. 7). The burial time is unconstrained above ca. 1 Myr.

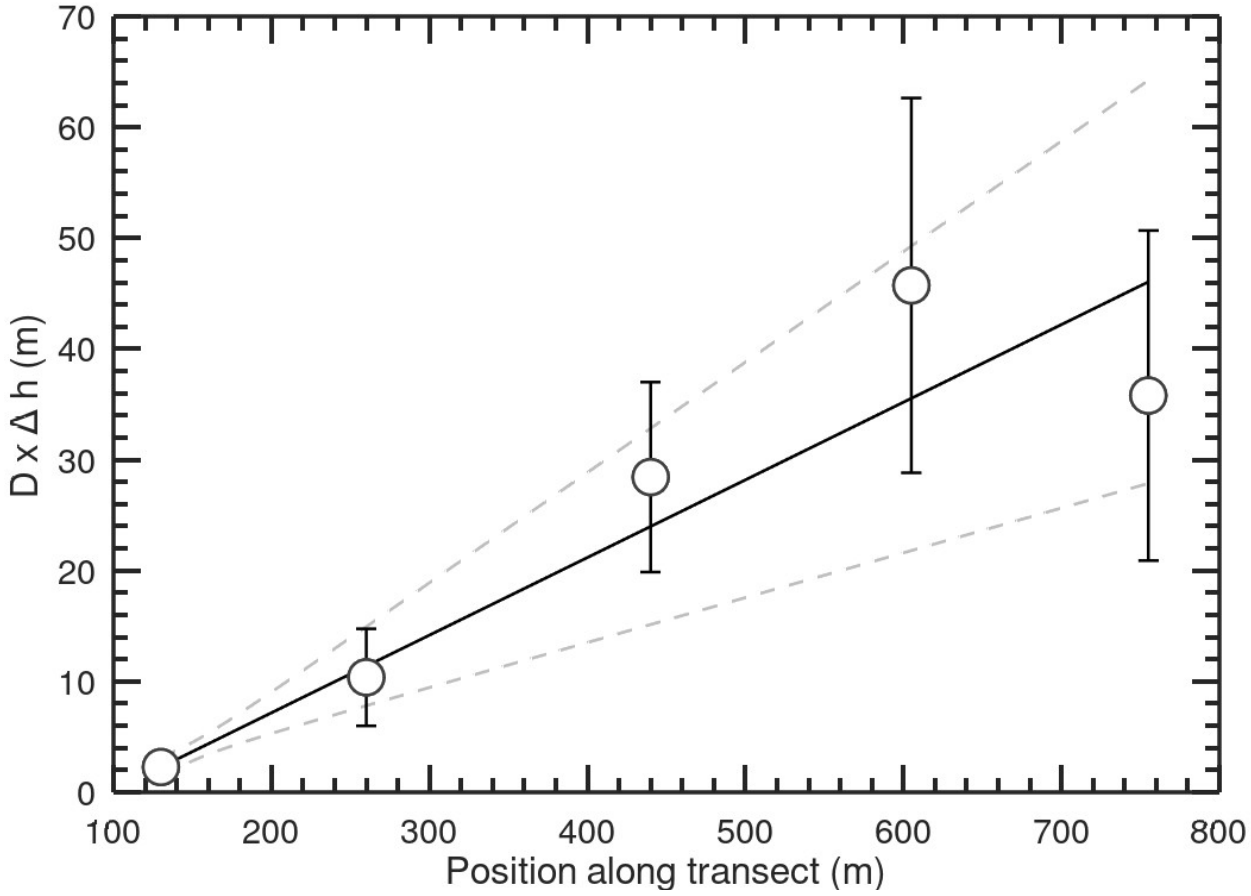

Figure S.5: Plot of the product of modeled peat depth (*D*) and surface/hydraulic head gradient (*Δh*) at LS1-LS5 vs. the downslope position along the transect. If the flow of water through the peat layer is dominated by horizontal flow because of the low permeability of the underlying clay-rich saprolite, and hydraulic conductivity within the peat layer is spatially uniform, then *D x Δh* should increase linearly along the downslope transect to accommodate a linear increase in discharge with distance from the drainage divide (main text, section 6.2). This behavior is observed, which supports that the modeled peat thickness are reasonable.

Figure S.6: Example photograph of a study soil pit (LS4).

Supporting Text S.1:

To calculate watershed-averaged denudation rates, we assume that the sampled stream sediment is derived from erosion of quartz-bearing saprolite on the hillslopes and that this material is then transported downslope through the peat layer, which functions as physically mobile regolith. We further assume that the peat layer is vertically mixed over the timescales of downslope transport. The change in the concentration of a cosmogenic nuclide, N, in quartz from the peat layer with time can then be described by the differential equation:

$$\frac{d\langle N\rangle}{dt} = \langle P\rangle[Qtz_{soil}] - \langle N\rangle\frac{E_{soil}}{z}[Qtz_{soil}] - \langle N\rangle\lambda[Qtz_{soil}] + N_{\text{sub}}\frac{E_{sap}}{z}[Qtz_{\text{sub}}] \qquad \text{Eq. S.1}$$

where $\langle P\rangle$ represents the depth-averaged ^{10}Be or ^{26}Al production rate in quartz in the peat layer (atoms g^{-1} yr^{-1}), $[Qtz_{peat}]$ and $[Qtz_{sap}]$ the concentrations of quartz in the peat layer and the saprolite, $\langle N\rangle$ the depth-averaged concentration of ^{10}Be or ^{26}Al in quartz in the peat layer (atoms g^{-1}), z the saturated peat layer mass-thickness (g cm^{-2}), λ the decay constant of ^{10}Be or ^{26}Al (yr^{-1}), N_{sap} the concentration of ^{10}Be or ^{26}Al in quartz at the top of the saprolite (atoms g^{-1}), and E_{sap} the erosion flux of saprolite (g cm^{-2} yr^{-1}). The first term on the right-hand side represents *in situ* production in the peat layer, the second term nuclide loss through erosion of the peat layer, the third nuclide loss through radioactive decay, and the fourth nuclide gain through erosion of saprolite.

For a mixed layer, the average production rate in the layer for production reactions that can be approximated as attenuating exponentially with depth is given by:

$$\langle P\rangle = \sum_i \frac{P_{0,i}\Lambda_i}{z}\left(1 - e^{\frac{-z}{\Lambda_i}}\right) \qquad \text{Eq. S.2}$$

where $P_{0,i}$ is the production rate at the surface by reaction i (atoms g^{-1} yr^{-1}) and Λ_i is the mean free path of the radiation responsible for that reaction (g cm^{-2}). If chemical weathering in the saprolite occurs below the penetration depth of most cosmic radiation, the concentration of ^{10}Be or ^{26}Al at the top of the saprolite (N_{sap}) is set by E_{sap} and by the mass-thickness of the peat layer (z):

$$N_{sap} = \sum_i \frac{P_i(0)}{\lambda + E_{sap}/\Lambda_i} e^{\frac{-z}{\Lambda_i}} \qquad \text{Eq. S.3}$$

The erosion rate of the saprolite can be related to the erosion flux from the peat layer using the conservation of mass of quartz, wherein the mass of quartz entering the peat layer from below must equal the mass leaving by physical erosion:

$$E_{\mathrm{sub}} = E_{soil}\frac{[Qtz_{soil}]}{[Qtz_{\mathrm{sub}}]} \quad \text{Eq. S.4}$$

Assuming steady state, substituting Eqs. S.2 through S.4 into S.1, and rearranging gives an expression for the ^{10}Be or ^{26}Al concentration in quartz as a function of E_{sap}, the peat layer thickness, and the enrichment of quartz across the saprolite-peat layer interface (R) (here Eq. S.5, main text Eq. 6):

$$\langle N \rangle = \sum_i \frac{P_i(0)\Lambda_i}{z}\left(1 - e^{\frac{-z}{\Lambda_i}}\right)\left[\frac{E_{sap}}{\rho h R} + \lambda\right]^{-1} + \frac{E_{sap}}{Rz}\frac{P_i(0)}{\left(\lambda + \frac{E_{sap}}{\Lambda_i}\right)}e^{\frac{-z}{\Lambda_i}}\left[\frac{E_{sap}}{zR} + \lambda\right]^{-1} \quad \text{Eq. S.5}$$

Supporting Text S.2:

The signal averaging timescales presented in Table 2 were calculated using the denudation rates for the hillslope transect positions determined from the Markov Chain Monte Carlo inversion as follows:

$$t_{avg} = \frac{1}{C_{Total}} \sum_i \frac{C_i}{\lambda_n + \frac{D}{\Lambda_i}} \quad \text{Eq. S.6}$$

where t_{avg} is the integration timescale of the signal, C_{Total} is the total cosmogenic nuclide concentration under the steady-state denudation rate, and C_i is the concentration attributable to production mechanism i. The summation is over all production functions.

Table S.1. Parameters for the site-specific muon model (main text, section 3.5.1).

Parameter	**P_1** at g^{-1} yr^{-1}	**P_2** at g^{-1} yr^{-1}	**P_3** at g^{-1} yr^{-1}	**P_4** at g^{-1} yr^{-1}	**Λ_1** g cm^{-2}	**Λ_2** g cm^{-2}	**Λ_3** g cm^{-2}	**Λ_4** g cm^{-2}
Nuclide								
Al-26	0.4540	0.0888	0.1651	0.0670	998	3175	1109	4304
Be-10	0.0440	0.0086	0.0203	0.0082	998	3175	1109	4304

Table S.2. Least-squares solutions to Eq. 5 for a constant overburden thickness.

ID	**LS2**	**LS3**	**LS4**	**LS5**
Thickness (g cm^{-2})	360	449	263	369
Denudation rate (t km^{-2} yr^{-1})	2.50	1.15	2.80	3.93